Energy & Buildings 306 (2024) 113924

Contents lists available at ScienceDirect

Energy & Buildings

journal homepage: www.elsevier.com/locate/enbuild

Influence of geometrical levels of detail and inaccurate material optical properties on daylight simulation

Nima Forouzandeh [a,*], Eleonora Brembilla [a], Liangliang Nan [b], Jantien Stoter [b], Alstan Jakubiec [c]

[a] Department of Architectural Engineering and Technology, Faculty of Architecture and the Built Environment, TU Delft, Netherlands
[b] Department of Urbanism, Faculty of Architecture and the Built Environment, TU Delft, Netherlands
[c] John H. Daniels Faculty of Architecture, Landscape and Design, University of Toronto, Canada

ARTICLE INFO

Keywords:
Interior
Digital twin
LOD
Digitization
Retrofit

ABSTRACT

Optimizing the built environment via simulations of building models hinges on standardizing data acquisition. In this research, we put forward distinct levels of detail for geometry and material inputs, specifically tailored for indoor daylight applications. We primarily focus on understanding the uncertainties arising from imprecise estimations of material optical properties and incomplete geometrical inputs in climate-based indoor daylight simulations. Employing a Monte Carlo approach, we analyzed six office and teaching spaces, creating 20 variations for each by altering geometrical completeness and material accuracy. The technique of excluding non-permanent objects below certain sizes in four graduated steps was used to derive and test the impact of various geometrical levels of detail. Our findings reveal that different levels of geometrical completeness lead to errors ranging from 1.08% to 18.05%. Additionally, a twofold increase in simulation time was noted when geometrical detail was enhanced relative to the most basic model. Errors stemming from imprecise definitions of material optical properties showed a normal distribution. The uncertainty in simulation outcomes showed a linear rise with increasing input material uncertainty, lying between 10% to 30%, depending on space configurations. We observed heightened uncertainty near openings, attributed to window transmittance effects. The research underscores that daylight predictions are markedly more sensitive to transmittance uncertainties than to those in reflectance, regardless of the window-to-floor ratio. These insights may help to guide a more efficient data acquisition process of indoor spaces for daylight simulations.

List of Acronyms
AHR Average Hemispherical Reflectance.
CBDM Climate-based Daylight Modeling.
DA Daylight Autonomy.
DDS Dynamic Daylight Simulation.
GLOD Geometrical Level of Detail.
LOD Level of Detail.
MAPE Mean Absolute Percentage Error.
MCOA Material Class of Accuracy.
OBB Oriented Bounding Box.
PE Percentage Error.
RMSE Root Mean Squared Error.
SA Sensitivity Analysis.
TAI Total Annual Illumination.
UDI Useful Daylight Illuminance.
UQ Uncertainty Quantification.
WFR Window to floor ratio.

1. Introduction

Achieving the desired levels of daylight is crucial for a healthy building design. Low exposure to daylight hinders the functioning of the occupants. It is proven that low levels of daylight engender symptoms of depressive disorder and seasonal affective disorder in the occupants [1]. Sufficient daylight is also shown to mitigate the progression of childhood myopia [2]. On the flip side, excessive exposure to daylight causes discomfort glare increases the risk of overheating. This is even more critical in buildings where occupants are confined indoors and do not have free access to the outdoors (e.g., hospitals and prisons [1]). Optimizing daylight levels in building design plays a significant role in promoting the well-being, health, and productivity of occupants, while

* Corresponding author.
E-mail addresses: n.forouzandeh@tudelft.nl (N. Forouzandeh), E.Brembilla@tudelft.nl (E. Brembilla), L.Nan@tudelft.nl (L. Nan), J.stoter@tudelft.nl (J. Stoter), alstan.jakubiec@daniels.utoronto.ca (A. Jakubiec).

https://doi.org/10.1016/j.enbuild.2024.113924
Received 20 September 2023; Received in revised form 30 November 2023; Accepted 17 January 2024
Available online 23 January 2024

also addressing potential drawbacks associated with both inadequate and excessive exposure to natural light.

To predict the daylight performance of buildings at the design stage, numerical evaluation of daylight provision and occupant comfort has become an indispensable part of the design process. This has been recognized by national and international standardization entities such as the European Committee for Standardization (CEN) [3], and building certification programs such as LEED, BREEAM, and WELL [4–6]. They all mandate acceptable levels of daylight to ensure environmental sustainability and to meet occupants' comfort, increasingly relying on Climate-based Daylight Modeling (CBDM) annual metrics.

Simulation models are not only predictors of newly designed interiors, but they can also be instrumental in post-occupancy evaluations of buildings. Such studies aim to provide evidence from existing buildings to inform the future generation of buildings, and to provide a ground for testing different retrofit strategies. Retrofitting existing buildings provides a significant opportunity to enhance building performance and reduce its energy use, by up to 84% [7]. Besides, the replacement of existing buildings by newly constructed buildings is not more than 1-3% per year [8]. Thus, retrofitting the existing building stock is one of the main ways of achieving sustainability in the built environment that attracts considerable attention from policymakers and building owners. Physics-based simulations are crucial tools for practitioners to achieve higher levels of occupant satisfaction while minimizing energy consumption. With daylight as a key performance aspect of indoor spaces, several researchers implemented simulation as a retrofit decision support tool to optimize the design of different elements within the indoor space. These elements include skylights [9], inner windows [10], partitions [11], and louver systems [12], or electric lighting systems [13]. Jradi et al. further proposed retrofit packages rather than focusing on only one component of the space [14].

Daylight models are also implemented as part of the buildings' digital twins and for active Model Based Control (MBC) systems. Digital twins involve five main parts. (1) A physical part that is the real-world object or space being represented virtually using the (2) virtual part, alongside the (3) connections which require data transfer from the physical part to the virtual representation with non-mandatory feedback component, (4) data, and (5) services, i.e., the action of controlling building element [15]. In the case of daylight models, this includes simulation and control decision-making modules. This has been partly approached by a few researchers. Tzempelikos et al. developed a Venetian blinds MBC system considering daylight provision, glare, and energy use. They employed three control strategies, (1) cut-off angle, (2) daylight redirection, and (3) glare-based control methods [16]. Similar approaches are employed for the control of roller shades and synchronized shading operation using a simplified model [17]. Luo et al. proposed an MBC system based on surrogate models [18]. Xie et al. [19] also proposed a data-driven model fitted on pre-simulated data for glare control of the buildings. A similar approach based on an adaptive neuro-fuzzy model was approached by Kurian et al. [20]. A comparative study of rule-based control systems and MBCs for double-skin facades, carried out by Gennaro et al. looked at systems based on simulation results to minimize heating and cooling loads based on Useful Daylight Illuminance (UDI). [21]. The functionality of MBC models for flexible double-skin facades was extended to the other domains of indoor performance indicators along with daylight, including Indoor Air Quality (IAQ), temperature, and energy by Catto et al. [22].

Regardless of the final application, there are uncertainties associated with daylight simulation models caused by inaccurate definitions of different model components including end-user interactions with buildings elements [23], sky model, geometry, and material optical properties [24]. As more and more aspects of building design and operation rely on virtual models, the robustness and accountability of such models become an essential requirement.

Despite the sheer importance of the knowledge of potential errors in daylight simulation outputs caused by inaccurate inputs, there are no thorough sensitivity analysis and uncertainty quantification studies carried out that encompass both geometry and material optical inputs. Brembilla et al. investigated the sensitivity of Climate-based Daylight Modeling (CBDM) results to the reflectance of different semantics, e.g., walls and floors [25]. They implemented the method of Morris for ranking the influence of each element relative to the others, as well as the non-linearity associated with each [26]. This is the only Sensitivity Analysis (SA) study done in the daylight domain, according to Pang et al. in their review on sensitivity analysis in the building performance field [27]. Concerning the influence of GLOD on CBDM,[1] the effects of interior modeling GLOD on the results have been barely investigated in previous works. To the best of our knowledge, the only related work modeled the exterior geometry in six different levels of detail by the inclusion of different semantics based on size at each LOD [28]. In the exterior domain, the propagation of positional errors in the estimation of the solar irradiation of building roofs is studied by Biljecki et al. based on TU Delft's LODs jointly with varying XY/Z accuracy levels to realistically model acquisition techniques [29]. This lack of knowledge on the interior domain is rooted in a lack of proper definitions for interior GLODs. The existing definitions are not useful for daylight performance simulation, since they are intended to suit other building-related applications such as natural disaster management services [30], area determination [31], and route visualization [32].

In this work, we fill these gaps by addressing two main objectives: (1) defining a generalizable and discretized framework for geometrical levels of detail and material classes of accuracy for application in indoor daylight models, and (2) measuring the errors caused by inaccurate characterization of material optical properties (MCOA) and geometrical representation of the space (GLOD). The idea of GLOD has been extensively studied and applied in urban-level 3D modeling of buildings to balance the acquisition and reconstruction cost concerning the desired application requirements[33,34]. The introduction of a similar framework for material properties is also crucial for the automation and efficient planning of daylight improvements in existing buildings. This work applies such a framework to give insight into the potential errors caused by implementing less accurate and cheaper material characterization methods to minimize the modeling costs depending on the desired application. Unlike previous studies that predominantly focused on exterior GLODs, our work extends the understanding of the impact of GLODs on Climate-based Daylight Modeling (CBDM) results within indoor spaces. The novelty of this project lies in the proposal of a tailored definition of GLOD specifically designed for indoor daylight applications, complemented by the introduction of the concept of Material Class of Accuracy (MCOA). This dual-focus approach fills the knowledge gap in the literature by advancing the understanding of the interplay between geometry and material optical inputs in daylight simulations. This provides insights for researchers and daylight practitioners and establishes a standardized framework for future studies on the automation and digitization of daylight models for existing built environments.

2. Methodology

In this section, we first introduce the case study spaces, followed by our definitions of GLOD and MCOA in sections 2.2 and 2.3, respectively. Subsequently, we introduce a GLOD-MCOA matrix for representing different levels of detail for each case study concerning material accuracy and geometrical completeness. We used a Monte Carlo simulation for this study, which is explained in detail in Section 2.4, followed by a description of the CBDM method, tool, and metric used for daylight simulation in Section 2.5. Finally, the measures of uncertainty are introduced in Section 2.6.

[1] CBDM is the calculation of any illuminance and/or luminance by using realistic sun and sky conditions derived from standardized climate data.

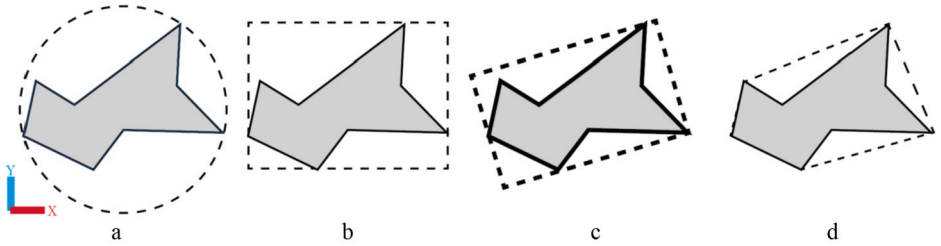

Fig. 1. Bounding geometries. From left to right: (a) Surrounding Sphere, (b) Axis-aligned bounding box, (c) Oriented Bounding Box (OBB), and (d) Convex hull.

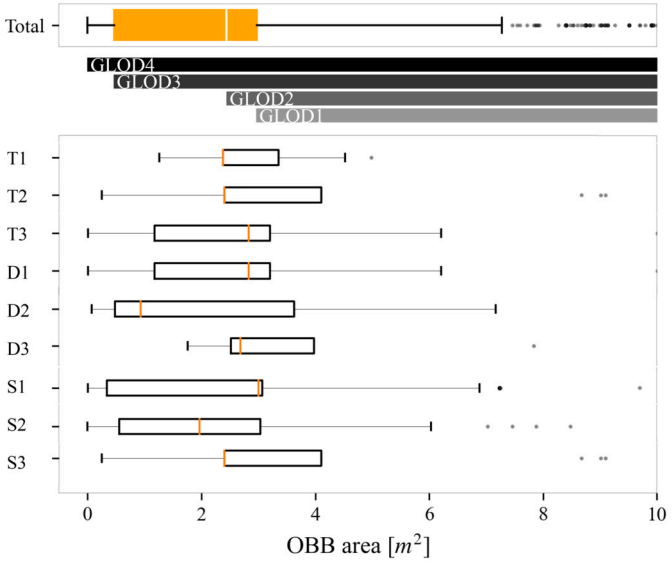

Fig. 2. Summary of object sizes in the case study spaces.

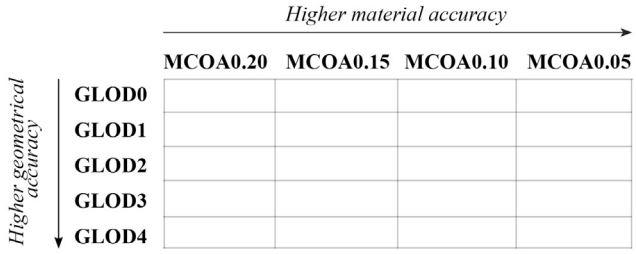

Fig. 3. The GLOD-MCOA matrix.

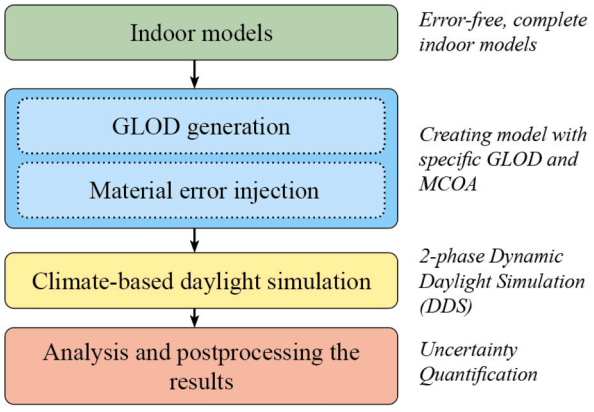

Fig. 4. Workflow of the uncertainty quantification study.

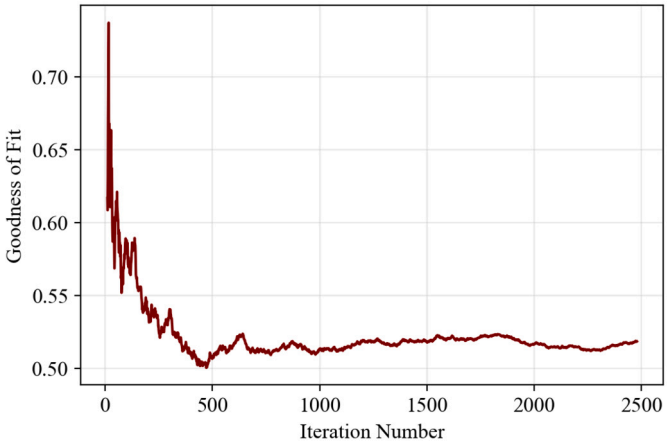

Fig. 5. Convergence experiment to determine the sufficient number of simulations (for space*D3* (MCOA0.2, GLOD4)).

Table 1
Case study spaces - general information.

Space ID	Location	Space type	Dimensions [m*m*m]	WFR [%]
T1	Toronto, CA	Classroom	14.5 * 9.7 * 3	9.6
T2	Toronto, CA	Classroom	16.6 * 10.6 * 3.5-6.7	9.1
T3	Toronto, CA	Classroom	11.7 * 8.3 * 4.0	14.1
D1	Delft, NL	Meeting room	5.8 * 4.4 * 5.8	9.1
D2	Delft, NL	Open office	12 * 9.8 * 5.8	29.4
D3	Delft, NL	Meeting room	7.2 * 3.4 * 2.6	40.9

2.1. Case study spaces and input preparation

We included six teaching and office spaces for our study. The general information and the 3D representation of the spaces are presented in Table 1 and Table 2, respectively. The spaces are sampled from common university spaces with varying sizes in three different geographical locations. Weather data are obtained from a repository of free climate data for building performance simulation [35]. We acquired the geometrical information using multiple LiDAR scans for each scene. Next, we registered all the scans and manually reconstructed the surface models for each space.

2.2. Geometrical Level of Detail (GLOD)

We define five GLODs by size-wise inclusion of non-permanent indoor objects. GLOD0 contains only the permanent objects, i.e., walls, windows, floor, and ceilings. These objects are the elements crucial for any type of indoor daylight simulation. The most complete GLOD is GLOD4, which contains all the indoor objects regardless of size. We defined three in-between GLODs by including objects greater than certain thresholds. These thresholds are determined as the surface area of Oriented Bounding Box (OBB) corresponding to the 25th, 50th, and 75th percentiles of the cumulative distribution of the non-permanent indoor objects across all of the case-study spaces. OBB is a geometric shape that is used to represent the smallest rectangular box that completely

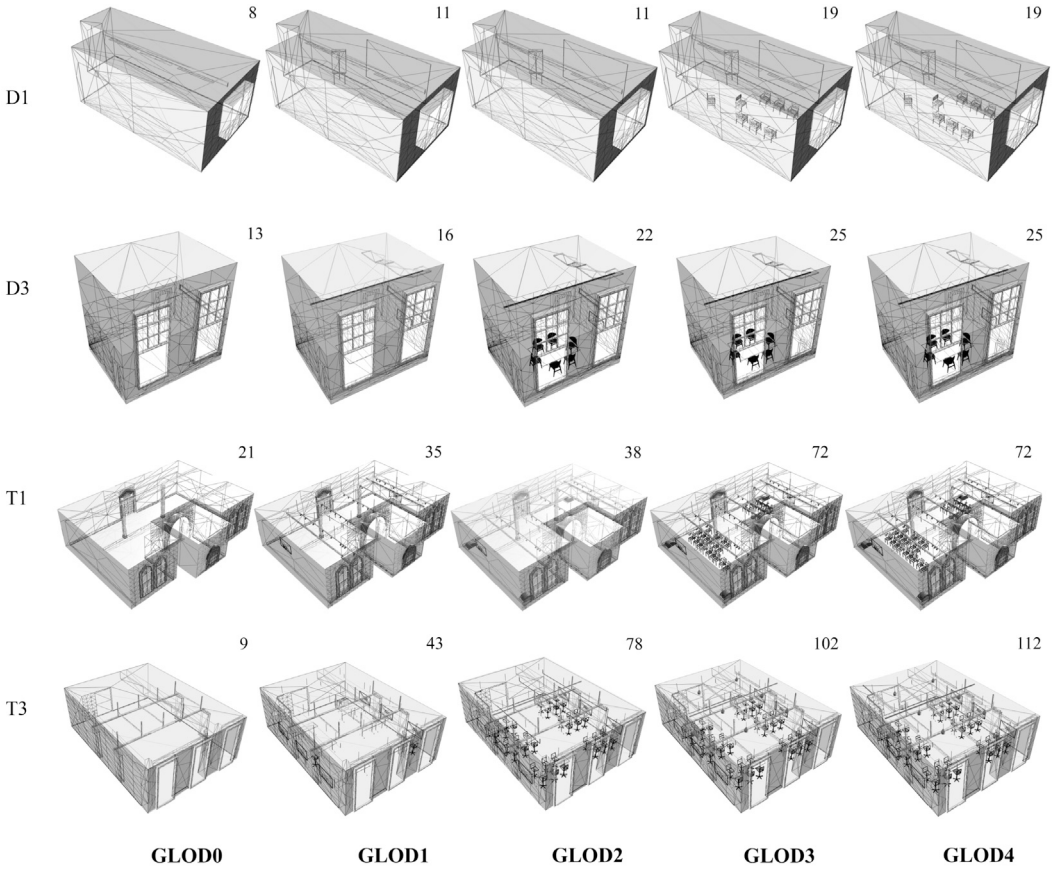

Fig. 6. 3D representation of spaces in multiple GLODs. The number of objects is indicated above each GLOD.

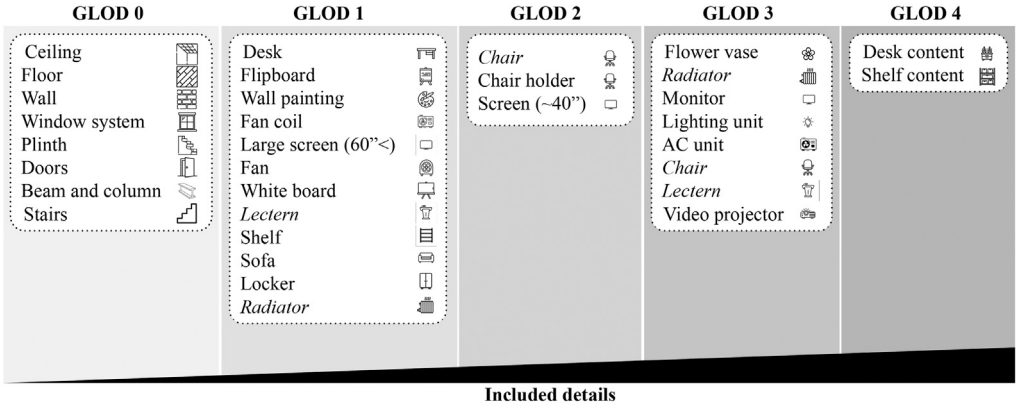

Fig. 7. The GLOD where each semantic first appears in the models. Some of the semantics appear in multiple GLODs for the first time, which are indicated in *italics*.

encompasses an object while allowing for arbitrary rotations in three-dimensional space. Unlike an axis-aligned bounding box (AABB), which is aligned with the coordinate axes, an OBB can be rotated to match the orientation of the object it surrounds. We chose OBB area instead of its volume because, in the input geometrical data, some of the indoor objects like desk surfaces are modeled as single surfaces instead of 3-dimensional volumes, while the volume for these objects is zero, they influence the daylight results and thus should be represented with a non-zero value. This measure is chosen for both its relative accuracy and generalizability. An example of four different bounding geometries in 2-dimensional space is shown in Fig. 1.

To increase the generalizability of our geometrical definition, three more interior spaces are included in the case study spaces that are only used for GLOD definition. These spaces are introduced in Table 3 and Table 4. These spaces are reused from another study done by Queck and Jakubiec on the calibration and validation of climate-based daylighting models based on one-time field measurement [36].

A statistical summary of object sizes in the case study spaces is presented in Fig. 2. According to this data, the threshold OBB area values for the in-between GLOD1, GLOD2, and GLOD3 are 3.0, 2.4, and 0.5 m^2, respectively. This means that, for instance, an object with OBB size of 2.2 m^2, appears in GLODs 3 and 4.

2.3. Material Class of Accuracy (MCOA)

There are several material characterization techniques used in daylight modeling practice. The most accurate one is the use of reflectance spectrophotometers. This method is not always feasible, leaving practitioners with other less accurate techniques for characterization, including luminance-illuminance reads, known as Average Hemispherical

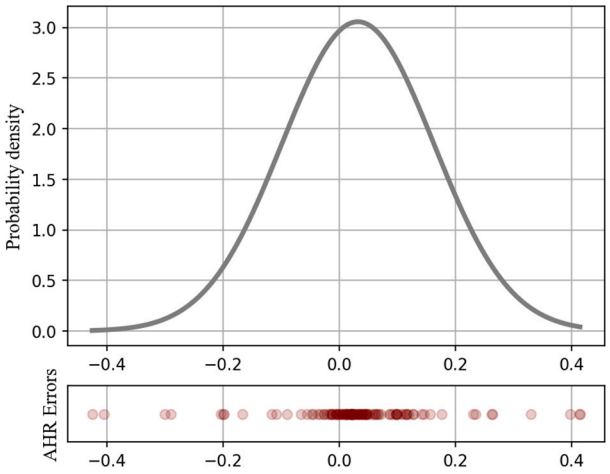

Fig. 8. Bell curve fitted to AHR errors, when compared against measurement from a reflectance spectrophotometer.

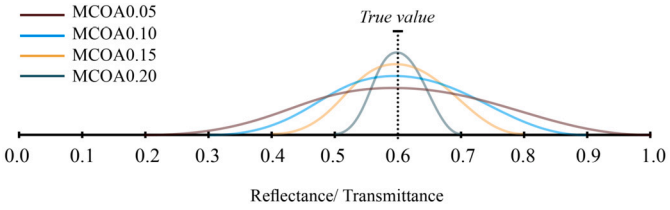

Fig. 9. An example of four MCOAs used in the Monte Carlo simulation. In this example the ground truth is 0.6. (For interpretation of the colors in the figure(s), the reader is referred to the web version of this article.)

Table 2
Case study spaces - 3D representation.

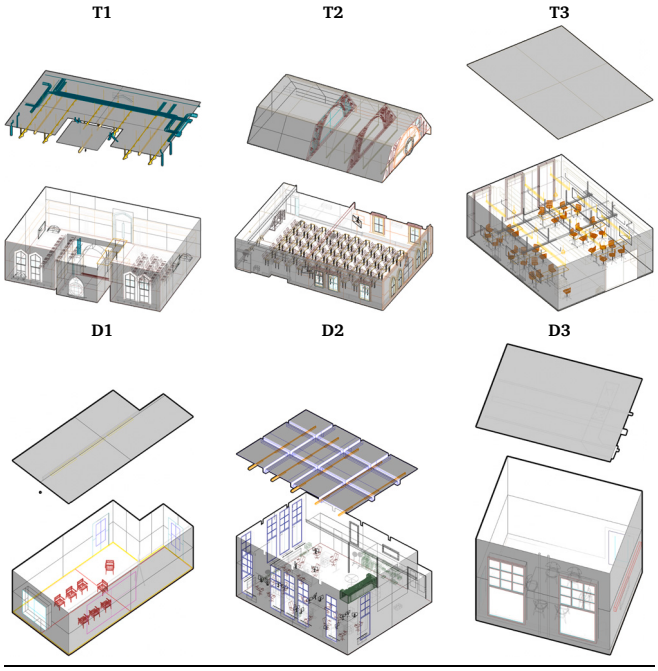

Reflectance (AHR), printed color charts, and suggested properties based on standards [3]. As for the transmittance of transparent materials, manufacturers typically provide designers with optical properties. However, a maintenance factor should be taken into account, which can considerably deviate from the value suggested by the manufacturer.

Table 3
Additional case study spaces for GLOD definition- general information.

Space ID	Location	Space type	Dimensions [m*m*m]	WFR [%]
S1	Singapore, SG	Open office	35 * 94 * 4.5	10.6
S2	Singapore, SG	Open office	26 * 30 * 3.3	33.1
S3	Singapore, SG	Open office	20.9 * 15.7 * 4.7	8.6

Table 4
Additional case study spaces for GLOD definition- 3D representation.

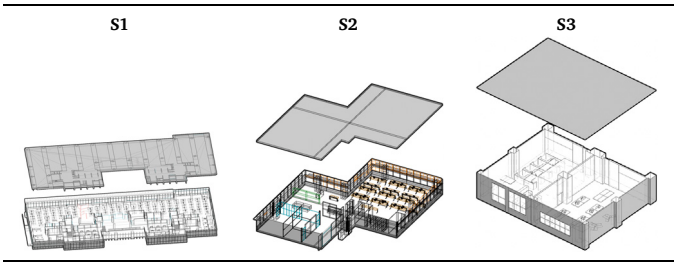

This deviation is context and configuration dependent [37]. Thus, an onsite measurement is suggested for accurate analysis.

To quantify the uncertainty associated with commonly measuring methods we measured a total of 106 building materials both using AHR, and reflectance spectrophotometer as ground truth. The AHR measurements were carried out using a Konica Minolta T-10A illuminance meter and a Konica Minolta LS-150 luminance meter. The ground truth measurements are done using a Konica Minolta CM-2600d reflectance spectrophotometer. Typical indoor materials, e.g., walls, floors, and interior furniture are included in these measurements under natural or electric lighting conditions.

A normal distribution was fitted to the results of the measurement errors. Based on the results, four different MCOAs are defined as incremental standard deviations. This was done so that the results of the study are generalizable to other material characterization techniques.

2.4. Monte Carlo simulation

For each space, we generated five different Geometrical Level of Detail as described in Section 2.2 and four Material Class of Accuracy as defined in Section 2.3. This results in a matrix of 20 models with different levels of material and geometrical detail and accuracy.

For each of the cells in the GLOD-MCOA matrix, we ran a Monte Carlo experiment. For each GLOD and MCOA combination, five hundred simulations were run. The number of simulations was determined based on a convergence test. For this, we calculated the Percentage Error (PE) for each run compared to the results corresponding to the model with error-free material properties. We then fitted a normal distribution to all the simulated cases. After each new run, the goodness of fit was tested using the Kolmogorov-Smirnov method and logged [38]. We observed that the goodness of fit converged to the range of 0.50-0.52 for *D3* (MCOA0.2, GLOD4) after 500 simulations as depicted in Fig. 5. This space was selected because of its small size, and thus lower computation load in high numbers. The choice of MCOA and GLOD was done such that the highest complexity and input variability are accounted for in this experiment. We used the same number for other spaces, GLODs, and MCOAs.

In total, we ran 10000 simulations for each case study, with 500 for each of the cells in the GLOD-MCOA matrix (Fig. 3), summing up to 60000 for all the spaces. The normality of the error distributions was tested with D'Agostino and Pearson's normality test which combines skew and kurtosis to produce an omnibus test of normality [39]. The overall workflow is depicted in Fig. 4.

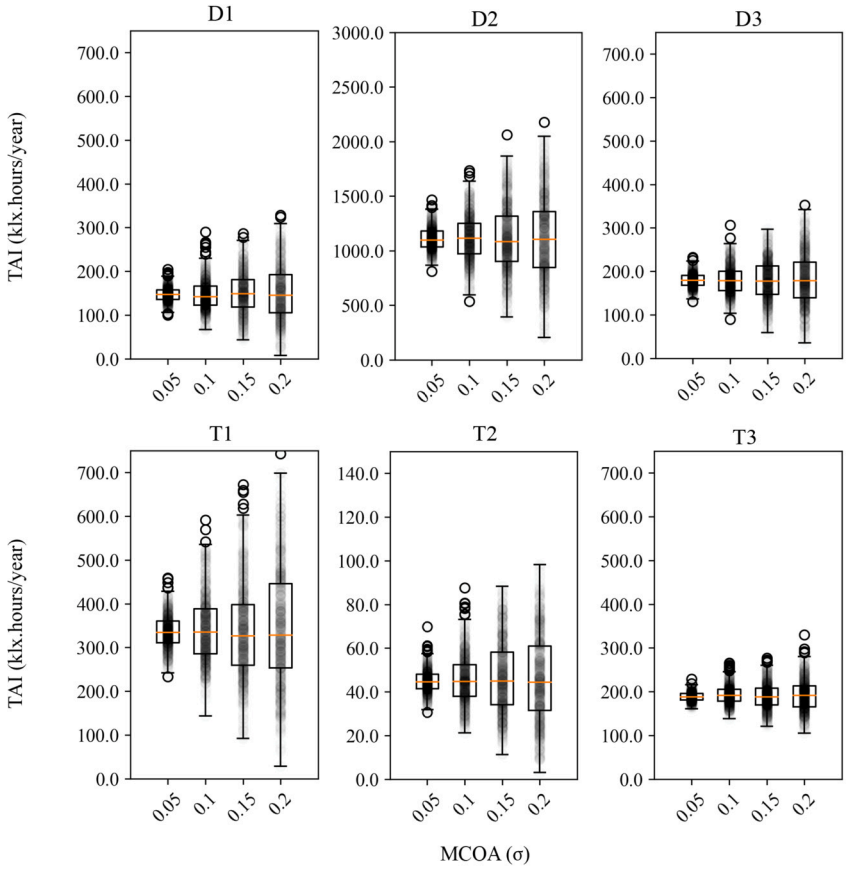

Fig. 10. TAI results based on GLOD 4. Boxplots show the interquartile values for one GLOD-MCOA combination. The highest and lowest 5 percentiles are considered and visualized as outliers. Note that the scales in the y-axis are different for *T2* and *D2* for better readability.

2.5. Daylight simulation

We used *Radiance* to conduct the indoor annual daylight simulation [40]. *Radiance* is a physically-based rendering system that is implemented in several building daylight simulation tools and is validated against measurements in many empirical studies [41,42]. In a validation study done by Mardaljevic on multiple indoor spaces, it is shown that *Radiance* predictions have a mean relative error of 5.6% with a standard deviation of 3.4% [43]. We used the Dynamic Daylight Simulation (DDS), which is based on the daylight coefficient methods and consists of the following steps [44]:

1. Performing annual daylight coefficient simulation ($C_{dc}S$).
2. Performing annual direct-only daylight coefficients simulation ($C_{dcd}S_d$).
3. Performing annual sun-coefficients simulation ($C_{sun}S_{sun}$).
4. Combining the results using the Eq. (1) to calculate the illuminance matrix (E).

$$E = C_{dc}S - C_{dcd}S_d + C_{sun}S_{sun} \tag{1}$$

We calculated the Total Annual Illumination (TAI) as the performance indicator for each run. This is calculated as the average illuminance value across the space throughout the occupied times in the entire simulation year. The occupancy hours are assumed between 9:00 and 17:00. Eq. (2) shows how TAI (in klx.hour/year) is calculated.

$$TAI = \frac{1}{1000 * G}\sum_{i=1}^{G}\sum_{j=1}^{H}(E_{ij}) \tag{2}$$

Where E_{ij} is the illuminance value at the point i at the time step j, G is the number of grid points, and H is the number of simulation hours.

2.6. Error calculation and uncertainty measures

We computed the following quantities as errors, and the corresponding equations are stated in Appendix A.

- Percentage Error (PE) for Total Annual Illumination (TAI). This quantity is used for convergence study and determining the sufficient number of Monte Carlo simulations (Section 2.4). Moreover, it was used to study the distribution of the uncertainties in Section 3.5.
- Mean Absolute Percentage Error (MAPE) for Total Annual Illumination (TAI). This is used for quantifying the influence of MCOA uncertainty in Fig. 16 as calculated in Eq. (A.2).
- Root Mean Squared Error (RMSE) of the time-series annual simulation data averaged across the simulation results for each GLOD-MCOA combination. This measure was used for studying the linearity of uncertainty when MCOA varies (Section 3.5), to quantify the influence of varying GLOD (Section 3.4), the spatial distribution of the uncertainties (Fig. 17), and for isolation of error caused by transmittance and reflectance (Fig. 18).

3. Results

In this section, we first describe the classification of geometries and materials as per GLOD and MCOA definitions. Next, daylight availability of the spaces is presented both in terms of TAI values and its spread across all the simulation iterations and as UDI maps. The influence of varying GLODs is investigated and presented in Section 3.4. Finally, the influence of varying classes of accuracy in materials MCOA is presented in Section 3.5.

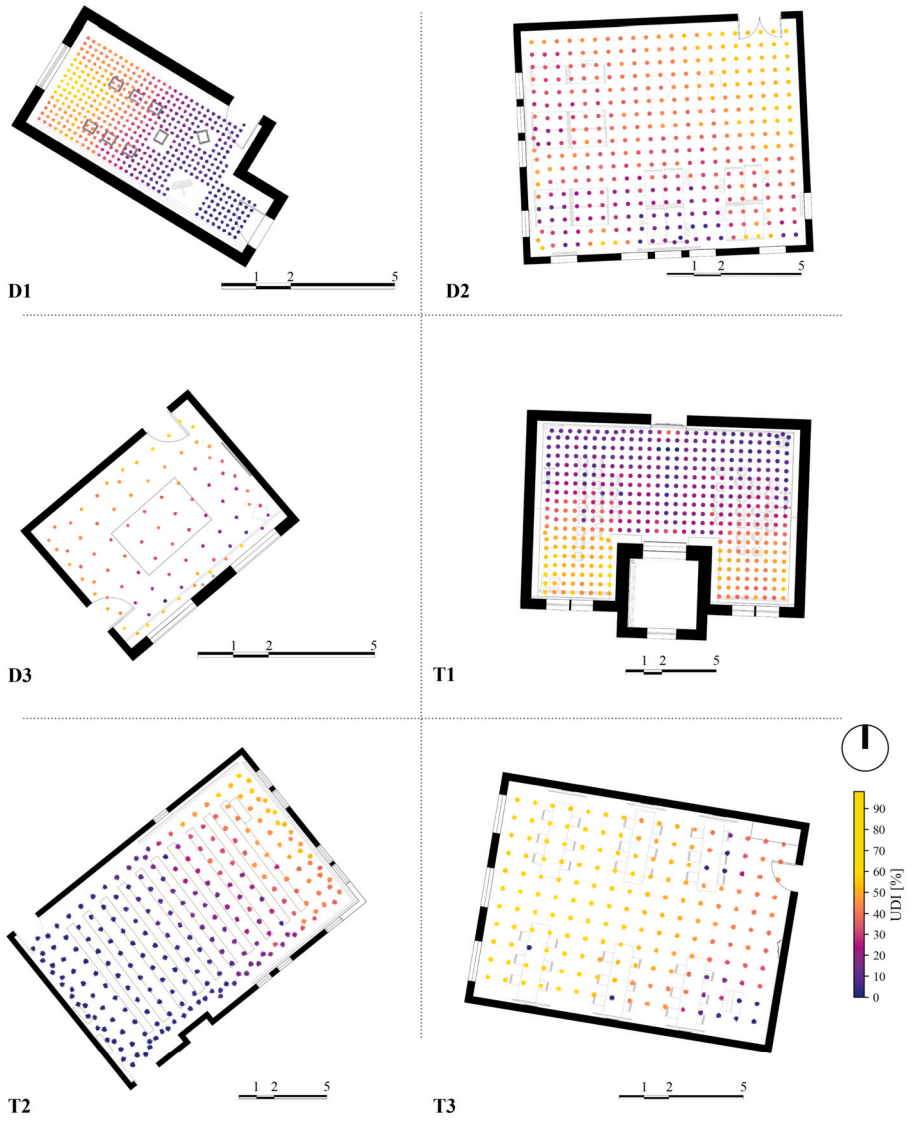

Fig. 11. UDI maps for the six spaces under evaluation. The considered UDI range is 300-3000 lx.

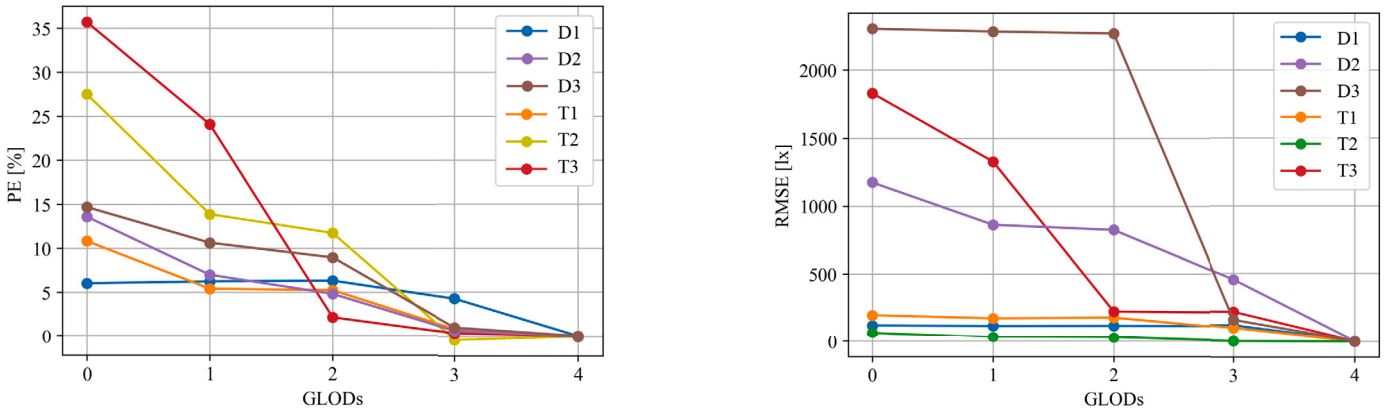

(a) PE (b) RMSE [lx]

Fig. 12. Influence of geometrical resolution on annual illuminance predictions.

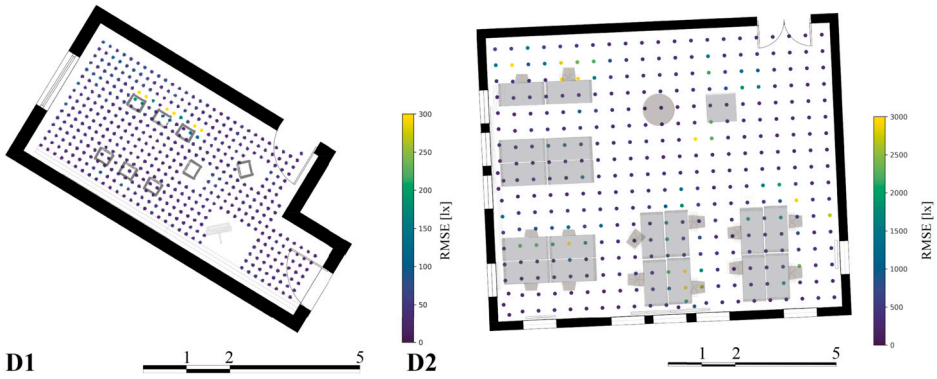

Fig. 13. Influence of geometrical resolution on annual daylight results - GLOD0 and GLOD4.

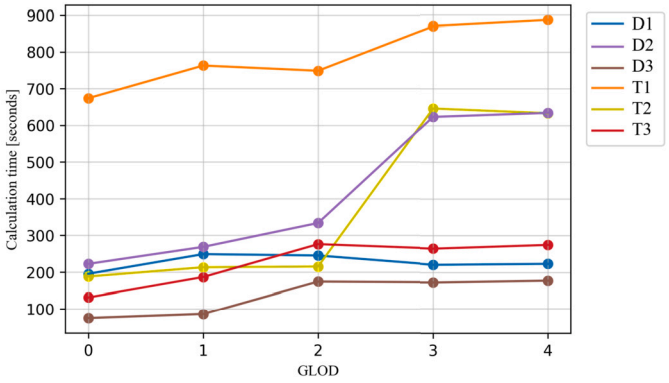

Fig. 14. Influence of geometrical resolution on simulation time.

Table 5
Influence of geometrical resolution on annual daylight results - RMSE and PE.

	GLOD0	GLOD1	GLOD2	GLOD3
		PE [%]		
min	6.04	5.42	2.16	0
max	35.67	24.07	11.75	4.25
mean	18.05	11.21	6.55	1.08
		RMSE [*lx*]		
min	57	894	50	44
max	949	51	876	841
mean	320	302	292	279

3.1. Geometrical Level of Detail (GLOD)

The 3D representation of three example spaces in multiple GLODs is shown in Fig. 6. Some of the semantics appear first in different GLOD across different interior spaces. This is because of the variation in the size of instances within that semantic. For instance, chairs appear first in GLOD3 for space *D1* and *T1*, but in *T3* and *D3* they appear in GLOD2. This is because their OBB sizes in these spaces are slightly larger than the former ones. A general pattern can be derived from the analysis of the nine indoor spaces included in this study, revealing the common semantic features found in each GLOD. This is illustrated in Fig. 7.

3.2. Material Class of Accuracy (MCOA)

The AHR measurement errors are plotted in Fig. 8. The errors are normally distributed with a standard deviation of 0.18 and a mean of 0.1. We chose reflectance and transmittance as the key material optical properties for uncertainty quantification. Specifically, we defined four material classes of accuracy as normal distributions with four spreads, represented by different standard deviations, from 0.05 to 0.2 as shown in Fig. 9. We selected these four accuracy levels to make the results of this study generalizable to any future approaches and scenarios with common optical properties of opaque and transparent surfaces.

3.3. Daylight availability in the studied spaces

Annual simulation results for the six indoor case study spaces are summarized in Fig. 10. According to the results in the most complete geometry case (GLOD4) and the most accurate material definition (MCOA0), median TAI ranges from 50 in *T2* to 1100 klx. hour/year in *D2*. This is due to the differences in orientation and WFR. In *T2*, the WFR is 9.5% and windows are mostly oriented towards North, while in *D2*, the WFR is 29.4% and the windows are oriented towards South and West. TAI values in other spaces fall within the results values in the above-mentioned spaces.

The distribution of the results seems symmetrical in all space variations with aligned medians within one space when changing MCOA. Thus the median TAI does not vary noticeably. Moreover, the spread of the TAI results increases consistently by an increase in uncertainty in material definitions across the spaces.

Besides TAI, Useful Daylight Illuminance (UDI) with 300-3000 lx thresholds (well-lit) is also calculated for all the grid points within each space. This is visualized in Fig. 11. According to this figure, higher daylight availability occurs in the grid points that are closer to the windows. In *D2* and *D3* those points receive higher levels of light than 3000 lx for the most portion of the occupancy hours. This is why these points are depicted in darker colors in these two case studies.

3.4. Influence of varying GLODs

Effects of varying GLODs are shown in terms of PE and RMSE in Fig. 12a and Fig. 12b, respectively. According to these results, on average, gradual exclusion of non-permanent objects in GLOD3 to GLOD0 results in 1.08, 6.55, 11.21, and 18.05% errors in the final TAI, respectively. The influence of geometrical resolution on annual daylight results is summarized in Table 5. Moreover, the spatial distribution of errors is plotted in Fig. 13. It shows that the results grid points around the furniture pieces have the highest deviations from the ground truth with varying GLODs.

The errors are correlated with the number of removed furniture pieces. The highest error happens in *T2* and *T3* with 27% and 36% respectively. This is due to the relatively higher furniture density in these spaces. The least errors are seen in *D1* and *T1* with 7% and 11% respectively. On average 18% error is observed in the six datasets when the non-permanent objects are completely removed from the model. This mean error is less than 5% in GLOD3 when desk and shelf content are not included in the model. In GLOD2, the errors are on average less than 10%. In these models, indoor objects including flower boxes, small radiators, monitors, lighting fixtures, AC units, chairs, lecterns, and video

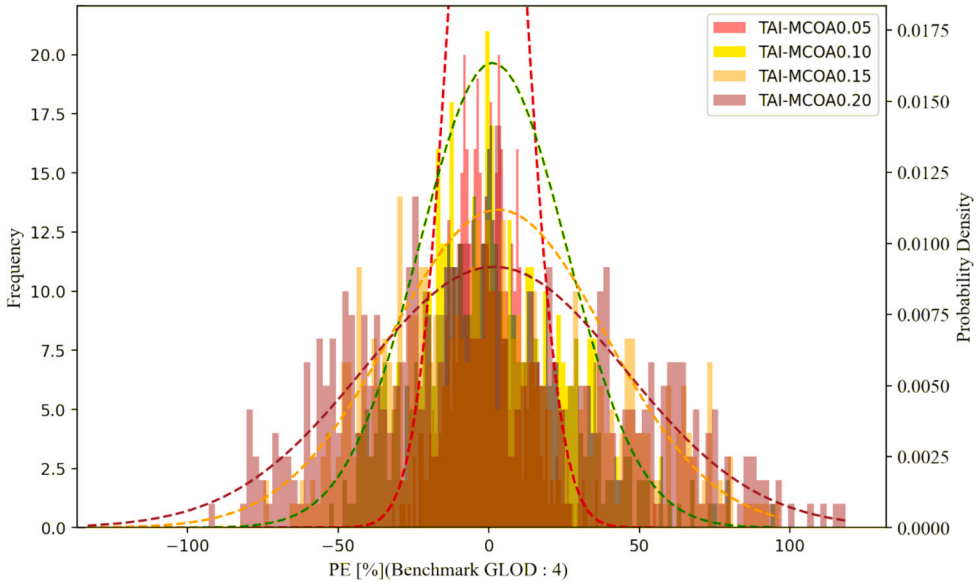

Fig. 15. Distribution of errors in the estimation of the TAI for space T2 with the four different MCOA and the fitted normal probability density functions for each one (*T2*).

projectors are excluded along with desk and shelf content. The resulting mean error in GLOD1 is around 15%. A steep increase in error can be seen in this step in space *T3*, which is possibly due to the high density of chairs that are removed in this GLOD (see Fig. 12a). A similar slope is seen in GLOD2 for space *T2*, where chairs are removed, and in GLOD0 where a high number of desks are removed from the model.

The impact of geometrical resolution on annual simulation time was also measured. As shown in Fig. 14, an increase in calculation time is evident across all the case study spaces. Simulation time is a function of complexity in the model which is partly due to the number of non-permanent objects included and partly due to the complexity of the object mesh. In all the spaces a decrease can be seen in the simulation time when this complexity is decreased. Between 25% (in *D1*) and around 200% (in *T2*, *D2*, and *D3*) was seen in the change in simulation time. Two different slope patterns can be seen here, firstly those of *T2* and *D2*, with a high slope on GLOD3, and that of the rest. This again can be attributed to the discrepancy in complexity of the models among the two groups.

3.5. Influence of varying MCOA

Fig. 15 shows the distribution of errors, as calculated in Eq. (A.1), in *T2* in GLOD4 and four different MCOAs. The distribution of errors seems to be symmetric, although in most MCOA-GLOD combinations it is not normal according to the results of the normality test, as presented for all the spaces in Appendix B, Table B.6.

Fig. 16 shows the uncertainties as calculated in Eq. (A.2) in all the six study spaces and GLODs. The benchmark Geometrical Level of Detail (GLOD) is GLOD4 for this error calculation. In the most complete model (GLOD4) in *D1*, *T1*, and *T2* the uncertainty ranges from 10% in MCOA0.05 to 35% in MCOA0.2. This range is slightly narrower in *D2* and *D3*, and is 8-30% in MCOA0.05 to MCOA0.2. In *T3*, a different trend is seen and the errors range from 5% for MCOA0.05 to 15% in MCOA0.2. Generally, the uncertainty in the prediction of the annual daylight simulation results linearly increases by an increase in the material uncertainty across all the spaces and GLODs. This was also observed in Fig. 10.

Fig. 17 shows a spatial analysis of the errors, from which we can see that the illuminance estimation uncertainty is larger around the glazing. This leads to the hypothesis that uncertainty in defining transmittance propagates into larger errors compared to reflectance. To further test this hypothesis, and to independently study the influence of uncertainty in reflectance and transmittance, for three spaces with three different WFR values, namely *D3* (WFR 40.9%), *T3* (WFR 14.1%), and *D1* (WFR 9.1%), we ran 8000 simulations with independent variations in reflectance and transmittance from MCOA0.5 to MCOA0.20. The uncertainty is calculated as described in Eq. (A.3) on the 16 MCOA combinations shown as crosses in Fig. 18. The uncertainty values are then interpolated across the 2D domain to study the trends. The result for *D1* and *D3* is horizontal gradients, showing the higher influence of transmittance uncertainty on illuminance prediction, while in *T3* the influence of reflectance is higher.

4. Discussion

Daylight models serve the purpose of evaluating daylight provision and visual comfort, applicable to both design and retrofit scenarios, as well as real-time digital twins and control systems. Geometrical model and material properties are the key inputs for Climate-based Daylight Modeling. In this study, we measured the impact of systematically injecting errors in these two inputs on the annual simulation results to decide on the best data modeling approach (i.e., to reconstruct models that are detailed enough to produce acceptable outcomes but that do require the least performance and modeling investment). In the following subsections, results concerning the definition of discretized levels are discussed first, followed by a discussion on the results for material properties. Overall limitations of the present work are then addressed in a subsequent section.

4.1. Geometrical Level of Detail (GLOD)

During the post-occupancy phase of a building's life cycle, the fundamental structures of the space, such as walls, windows, ceilings, and floors, remain unchanged, while non-permanent objects can be modified as needed. Therefore, our focus was on these non-permanent objects when defining the levels of detail in geometry (GLOD). In addition, this may also provide us insights into the impact of the geometry of permanent objects. The GLOD definition was based on data-driven size thresholds, determining which objects to include or exclude. The results indicate that GLOD2 models result in less than a 15% error in daylight availability simulations. This suggests that removing objects with an OBB size smaller than 2.4 m^2 will have a minimal negative impact on

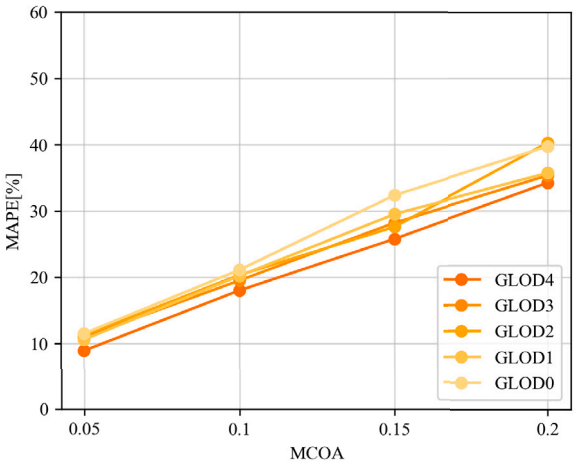

(a) *D1*

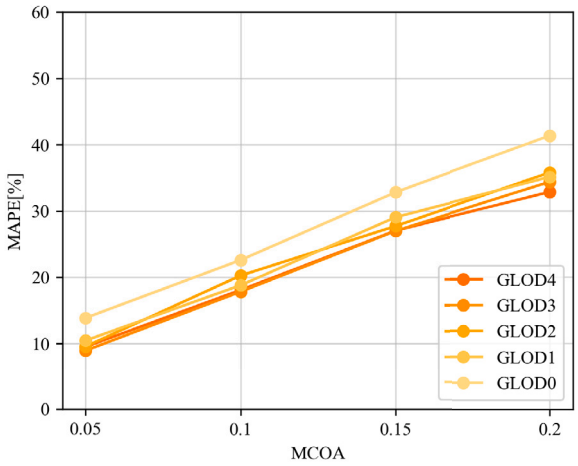

(b) *T1*

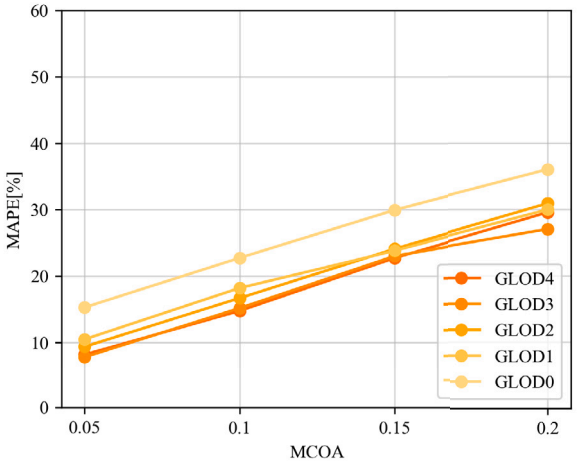

(c) *D2*

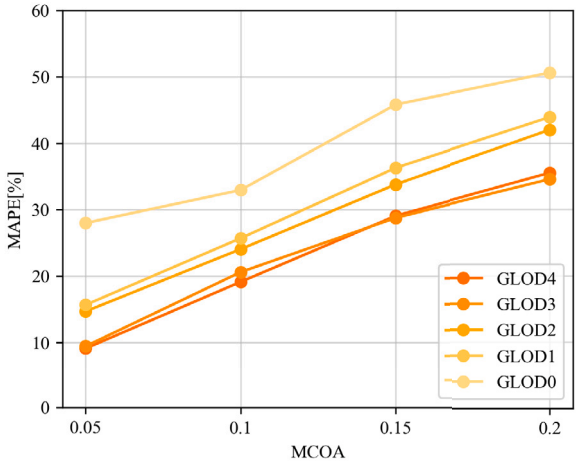

(d) *T2*

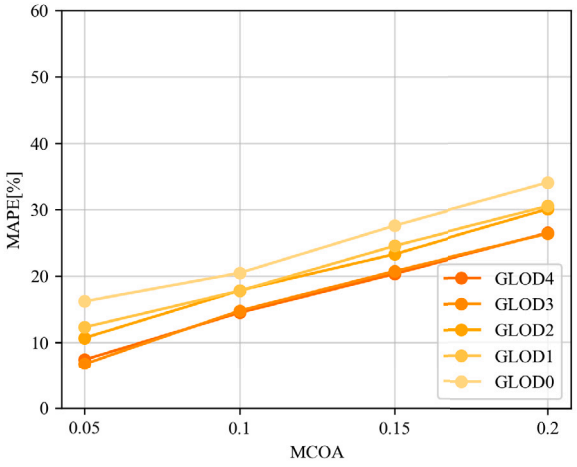

(e) *D3*

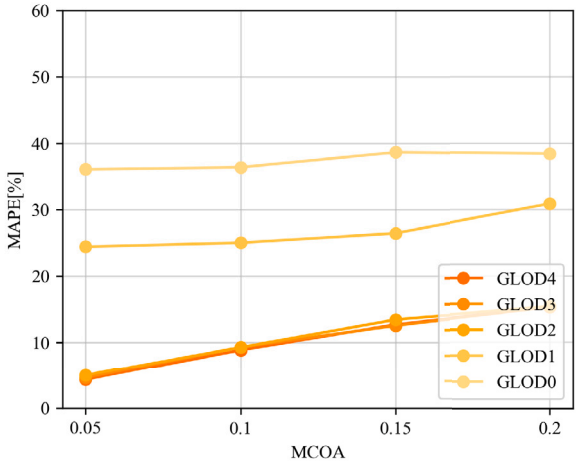

(f) *T3*

Fig. 16. Influence of varying MCOA.

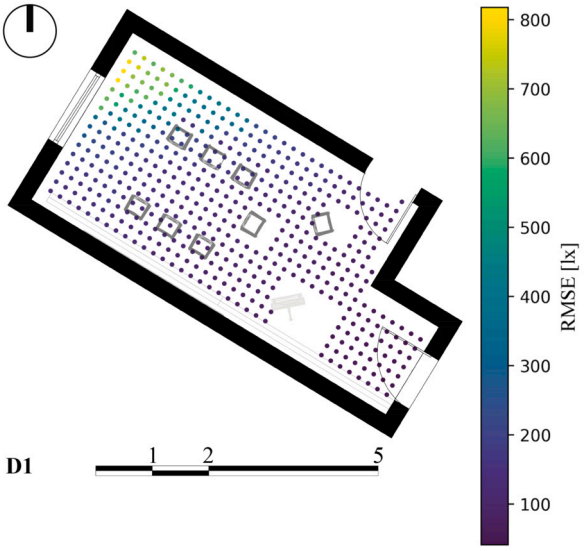

Fig. 17. Spatial distribution of prediction errors caused by inaccurate material definition (MCOA0.2-GLOD4–D1).

the output results. Such objects may include desks, shelf contents, AC units, certain chairs and lecterns, small radiators and flower boxes, and video projectors (refer to Fig. 7).

There are mainly two ways of defining GLODs, one being the gradual inclusion of non-permanent objects, and the other being a reduction of geometrical complexity using mesh simplification techniques such as reduction, collapsing, or amalgamation. In this study, we focused on the former approach, since we find it more probable to be chosen by practitioners. However, the latter is likely the reason why no correlation can be observed between TAI PE and the drop in the simulation times (see Fig. 12 and Fig. 14).

The OBB size of the non-permanent objects was chosen as the primary basis for the definition of the GLODs in this study. This quantity was used as a criterion to gradually remove objects from the 3D scene and calculate the errors that resulted from this incomplete model. The fundamental motivation for employing this value was that it could be applied to other geometrical data, including point clouds of objects that exhibit excessive geometric details. It is a constrained definition, though, as it ignores factors like object orientation and proximity to windows. A more robust definition may also include the aspect ratio of the OBBs as well as its orientation. This will be further developed in the future work.

4.2. Material Class of Accuracy (MCOA)

The material optical properties were defined as a randomly picked value from a normal distribution centered around the ground truth. Four different distributions were used to represent four classes of material accuracy (MCOA). We based this definition on 106 measurements of opaque materials using a luminance/illuminance measurement method (also referred to as Average Hemispherical Reflectance (AHR)). Other common techniques of characterizing opaque materials, e.g., using reflectance spectrophotometer, illuminance-proxy [45,46], and CIBSE color charts are assumed to fall within the same ranges, with, for instance, reflectance spectrophotometer in MCOA0.05.

We generalized the results obtained for these opaque surfaces to transparent materials. The optical properties of transparent materials are commonly characterized by the manufacturer's data. However, depending on the context of the building, a maintenance factor is necessary to be applied to the nominal transmittance information [47]. Since the data was limited on the transparent materials and the potential inaccuracies caused by different characterization methods and wrongly assumed maintenance factors, we consistently applied the material definition of the opaque surfaces to transparent ones. In reality, the characterization of transparent and opaque materials is typically done using independent methods. If similar measured databases were accessible, it would allow for more accurate modeling of accuracy classes for transparent materials.

4.3. Limitations

The definition of GLODs in our study is unidimensional, i.e. only based on the Oriented Bounding Box (OBB) size of the non-permanent objects. This definition could be more complete if other descriptors of the objects, e.g. their semantic information were considered. Moreover, only non-permanent objects are considered for defining discretized GLODs, and the accuracy in modeling the main structures of the space, e.g., walls, floors, and ceilings is not studied. Also, regarding material optical properties, the classes of accuracy for both opaque and transparent materials are defined based on measurements of opaque surfaces. A similar thorough measurement of the transparent surfaces would complement the suggested framework.

In this study, we conducted all experiments numerically without on-site validation. This lack of ground truth measurement was mainly because of the unavailability of the spaces for long periods since they were all in-use office spaces or classrooms. Moreover, a lack of sufficient measurement resources hindered conducting a thorough validation study. Our assumptions are grounded in previously conducted validation studies on the rendering engine we employed, which indicated errors within 13%. However, conducting a validation study for our specific cases would further ensure the validity of our findings.

5. Conclusion

In this study, we have quantified the influence of incomplete geometrical modeling and inaccurate material definition on annual daylight predictions. We define Geometrical Level of Detail (GLOD) and Material Class of Accuracy (MCOA) for this study derived from measurements of in-use university and office spaces.

Exclusion of non-permanent objects in GLOD3-GLOD0 causes on average 1.08, 6.55, 11.21, and 18.05% errors in the output TAI values respectively. The errors are highest around the location of non-permanent objects in the room. However, excluding the non-permanent objects is shown to make the simulation run up to threefold faster. The errors arising from inaccurate definitions of material optical properties exhibit a normal distribution. Additionally, the uncertainty in measurements linearly increases with higher levels of input material uncertainty by 10-30% depending on the space. Notably, the uncertainty is more pronounced around the openings. This can be attributed to the fact that the overall uncertainty is primarily influenced by the uncertainty in the transmittance of materials.

The results of this study are useful for evaluating the novel methods of material characterization and geometrical reconstruction for daylight simulation, giving insights into the potential propagation of errors caused by inaccurate modeling of key daylight simulation inputs, such as material optical properties and (semi-)automatic geometrical reconstruction. Proper geometrical levels of detail and material classes of accuracy can be determined according to the available resources and the acceptable accuracy for a particular application. This research lays the ground for quantitative assessment of potential errors by novel material characterization and geometrical reconstruction methods. In general, for coarse daylight assessments of the buildings, e.g. at a regional/urban level, lower MCOA and GLODs could be deemed acceptable. However, for specific design indoor decision-making problems, higher MCOA and GLODs will result in more reliable solutions. In future studies, it is essential to continue exploring and refining automation in these processes

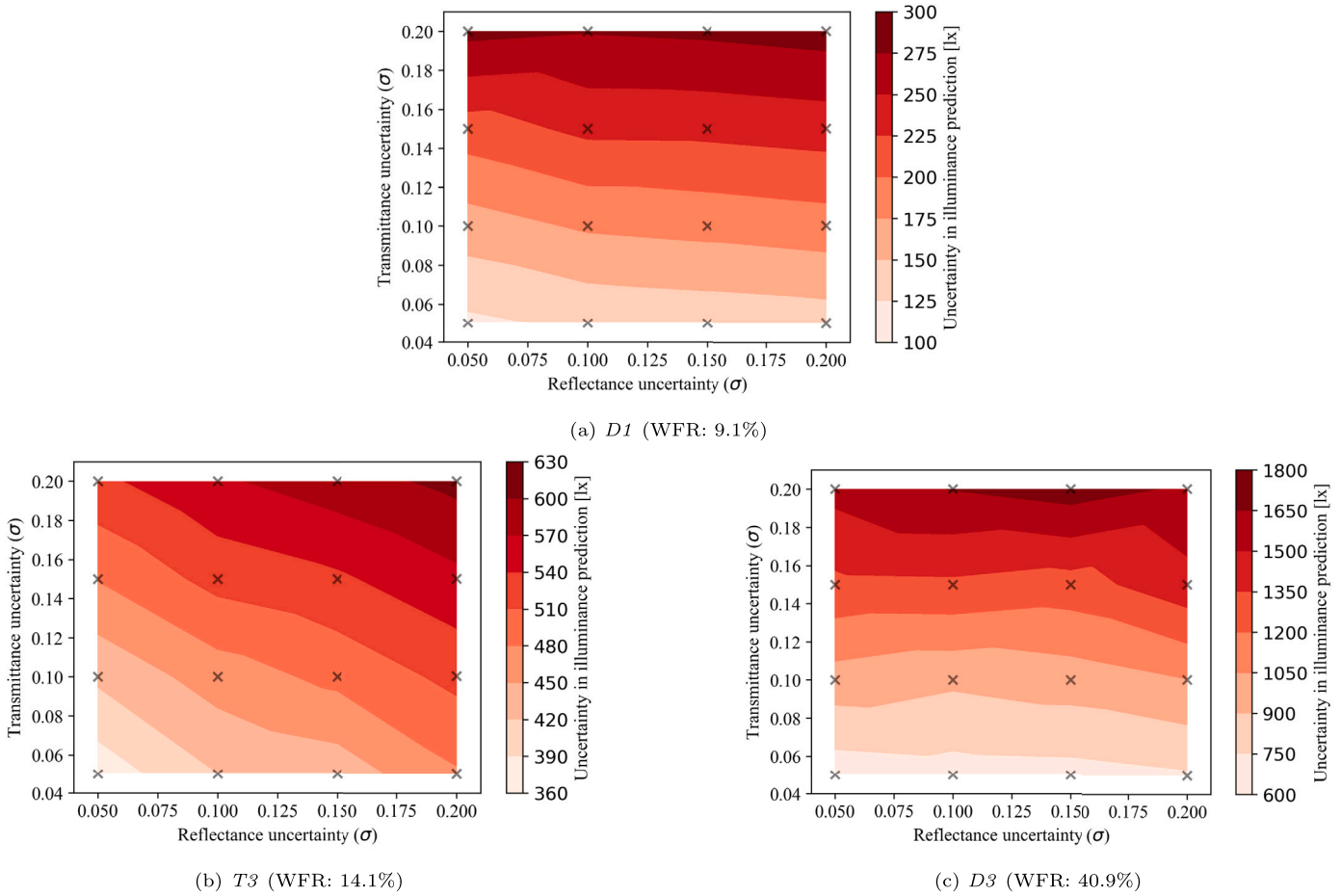

(a) *D1* (WFR: 9.1%)

(b) *T3* (WFR: 14.1%)

(c) *D3* (WFR: 40.9%)

Fig. 18. Uncertainty in the calculation of annual grid-based illuminance values. Crosses represent the uncertainty as calculated in Eq. (A.3). Gradient colors represent the interpolated uncertainty across the 2D domain of 0.05-0.20 reflectance-transmittance independent uncertainties.

to enhance the efficiency and accuracy of daylight simulations using digital building models.

CRediT authorship contribution statement

Nima Forouzandeh: Conceptualization, Data curation, Formal analysis, Investigation, Methodology, Software, Visualization, Writing – original draft, Writing – review & editing. **Eleonora Brembilla:** Conceptualization, Funding acquisition, Project administration, Resources, Supervision, Writing – review & editing. **Liangliang Nan:** Supervision, Writing – review & editing. **Jantien Stoter:** Project administration, Resources, Supervision, Writing – review & editing. **Alstan Jakubiec:** Funding acquisition, Project administration, Resources.

Declaration of competing interest

The authors declare that they have no known competing financial interests or personal relationships that could have appeared to influence the work reported in this paper.

Data availability

Data will be made available on request.

Appendix A. Measures of uncertainty

- Percentage Error (PE) for Total Annual Illumination (TAI).

$$100 * \frac{(TAI_i - TAI_{bm})}{TAI_{bm}} \tag{A.1}$$

Where:
- TAI_i is Total Annual Illumination, and
- TAI_{bm} is TAI for the benchmark model.

- Mean Absolute Percentage Error (MAPE) for TAI.

$$\frac{100}{N} * \left|\frac{(TAI_i - TAI_{bm})}{TAI_{bm}}\right| \tag{A.2}$$

Where:
- N is the number of iterations in the corresponding GLOD and MCOA.

- Average Root Mean Squared Error (RMSE) of the time-series annual simulation data:

$$\frac{1}{N}\sum_{i=1}^{N}\sqrt{\frac{1}{H*G}\sum_{j=1}^{H}\left(\sum_{k=1}^{G}(x_{ijk}-\hat{x}_{ijk})^2\right)} \tag{A.3}$$

Where:
- H represents the total number of occupancy hours between 8:00 and 17:00 throughout the year.
- G is the total number of grid points within a space.
- x_{ijk} denotes the illuminance value on the point k at time j in the i^{th} inaccurate iteration, and
- $\hat{x}_{ijk}$ represents the benchmark value for the same point in time and space.

Appendix B. Results of the normality test

Table B.6
Results of the normality test (p-value), normal distributions with p-values higher than 0.05 are highlighted with (*).

Space ID	GLOD	MCOA0.05	MCOA0.10	MCOA0.15	MCOA0.20
D1	4	0.006	0.000	*0.216	0.017
	3	*0.451	0.000	0.003	0.000
	2	*0.470	0.002	0.000	0.001
	1	*0.373	0.000	0.000	0.001
	0	*0.433	0.003	0.000	0.000
T1	4	0.016	*0.076	0.001	0.001
	3	0.015	0.000	0.002	0.004
	2	0.008	0.003	0.000	0.000
	1	*0.111	0.000	0.001	0.015
	0	*0.126	0.008	0.000	0.002
T2	4	0.000	0.000	0.000	0.000
	3	0.002	0.003	0.001	0.000
	2	0.004	0.009	0.000	0.000
	1	*0.092	0.006	0.000	0.000
	0	0.002	0.000	0.000	0.000
T3	4	*0.131	0.000	0.010	0.004
	3	0.005	0.000	0.005	0.000
	2	*0.511	0.003	0.003	0.000
	1	*0.056	0.000	0.001	0.000
	0	0.002	0.010	0.005	0.000
D2	4	0.001	*0.482	0.026	0.001
	3	*0.121	0.008	0.000	0.018
	2	*0.430	0.295	0.001	0.000
	1	*0.320	*0.106	0.021	0.002
	0	*0.760	0.004	0.002	0.001
D3	4	0.001	*0.483	0.027	0.001
	3	*0.121	0.008	0.000	0.018
	2	*0.438	*0.295	0.001	0.000
	1	*0.321	*0.107	0.022	0.002
	0	*0.763	0.005	0.002	0.002

References

[1] P. Tregenza, M. Wilson, Daylighting: Architecture and Lighting Design, Routledge, 2013.
[2] R. Chakraborty, L.A. Ostrin, D.L. Nickla, P.M. Iuvone, M.T. Pardue, R.A. Stone, Circadian rhythms, refractive development, and myopia, Ophthalmic Physiol. Opt. 38 (3) (2018) 217–245.
[3] EN 17037: Daylight in buildings, European Committee for Standardization, https://www.en-standard.eu/csn-en-17037-daylight-of-bui%ldings/, 2018.
[4] U.G.B. Council, Leed v4 for Building Design and Construction, USGBC Inc, 2014.
[5] BREEAM – Building Research Establishment Environmental Assessment Method, https://www.breeam.com/, July 2023. (Accessed July 2023).
[6] Standard | well V2, https://v2.wellcertified.com/v/en/concepts, July 2023. (Accessed July 2023).
[7] C. Regnier, K. Sun, T. Hong, M.A. Piette, Quantifying the benefits of a building retrofit using an integrated system approach: a case study, Energy Build. 159 (2018) 332–345.
[8] Z. Ma, P. Cooper, D. Daly, L. Ledo, Existing building retrofits: methodology and state-of-the-art, Energy Build. 55 (2012) 889–902.
[9] Y. Bian, J. Luo, J. Hu, L. Liu, Y. Pang, Visual discomfort assessment in an open-plan space with skylights: a case study with poe survey and retrofit design, Energy Build. 248 (2021) 111215.
[10] W.S. Koh, H. Liu, S. Somasundaram, S.R. Thangavelu, A. Chong, K. Pillai, H. Kojima, Y. Mori, Evaluation of glazing retrofitting solution for the tropics, Energy Build. 223 (2020) 110190.
[11] N. Abdollahzadeh, M. Tahsildoost, Z.S. Zomorodian, A method of partition design for open-plan offices based on daylight performance evaluation, J. Build. Eng. 29 (2020) 101171.
[12] A. Hashemi, Daylighting and solar shading performances of an innovative automated reflective louvre system, Energy Build. 82 (2014) 607–620.
[13] X. Zhou, D. Yan, T. Hong, X. Ren, Data analysis and stochastic modeling of lighting energy use in large office buildings in China, Energy Build. 86 (2015) 275–287.
[14] M. Jradi, C. Veje, B.N. Jørgensen, Deep energy renovation of the mærsk office building in Denmark using a holistic design approach, Energy Build. 151 (2017) 306–319.
[15] F. Jiang, L. Ma, T. Broyd, K. Chen, Digital twin and its implementations in the civil engineering sector, Autom. Constr. 130 (2021) 103838.
[16] J. Xiong, A. Tzempelikos, Model-based shading and lighting controls considering visual comfort and energy use, Sol. Energy 134 (2016) 416–428.
[17] I. Konstantzos, A. Tzempelikos, Y.-C. Chan, Experimental and simulation analysis of daylight glare probability in offices with dynamic window shades, Build. Environ. 87 (2015) 244–254.
[18] Z. Luo, C. Sun, Q. Dong, J. Yu, An innovative shading controller for blinds in an open-plan office using machine learning, Build. Environ. 189 (2021) 107529.
[19] J. Xie, A.O. Sawyer, Simulation-assisted data-driven method for glare control with automated shading systems in office buildings, Build. Environ. 196 (2021) 107801.
[20] C. Kurian, S. Kuriachan, J. Bhat, R. Aithal, An adaptive neuro-fuzzy model for the prediction and control of light in integrated lighting schemes, Light. Res. Technol. 37 (4) (2005) 343–351.
[21] G. Gennaro, F. Goia, G. De Michele, M. Perino, F. Favoino, Embedded singleboard controller for double skin facade: a co-simulation virtual test bed, in: Proceedings of International Conference of Building Performance Simulation Association BS2021, 1-3 Sep., 2021.
[22] E.C. Lucchino, F. Goia, Multi-domain model-based control of an adaptive façade based on a flexible double skin system, Energy Build. 285 (2023) 112881.
[23] E.S. Lee, E.S. Claybaugh, M. LaFrance, End user impacts of automated electrochromic windows in a pilot retrofit application, Energy Build. 47 (2012) 267–284.
[24] N. Kunwar, K.S. Cetin, U. Passe, Calibration of energy simulation using optimization for buildings with dynamic shading systems, Energy Build. 236 (2021) 110787.
[25] E. Brembilla, C.J. Hopfe, J. Mardaljevic, Influence of input reflectance values on climate-based daylight metrics using sensitivity analysis, Journal of Building Performance Simulation 11 (3) (2018) 333–349, https://doi.org/10.1080/19401493.2017.1364786.
[26] F. Campolongo, J. Cariboni, A. Saltelli, An effective screening design for sensitivity analysis of large models, Environ. Model. Softw. 22 (10) (2007) 1509–1518.
[27] Z. Pang, Z. O'Neill, Y. Li, F. Niu, The role of sensitivity analysis in the building performance analysis: a critical review, Energy Build. 209 (2020) 109659.
[28] R. Sadeghi, R. Mistrick, The impact of exterior surround detail on daylighting simulation results, Leukos 18 (3) (2022) 341–356.
[29] F. Biljecki, H. Ledoux, J. Stoter, An improved LOD specification for 3D building models, Computers, Environment and Urban Systems 59 (2016) 25–37.
[30] S. Kemec, S. Zlatanova, S. Duzgun, A new lod definition hierarchy for 3d city models used for natural disaster risk communication tool, in: Proceedings of the 4th International Conference on Cartography & GIS, vol. 2, Albena, June 2012, International Cartographic Association, 2012, pp. 17–28.
[31] R. Boeters, K. Arroyo Ohori, F. Biljecki, S. Zlatanova, Automatically enhancing citygml lod2 models with a corresponding indoor geometry, Int. J. Geogr. Inf. Sci. 29 (12) (2015) 2248–2268.
[32] B. Hagedorn, M. Trapp, T. Glander, J. Döllner, Towards an indoor level-of-detail model for route visualization, in: 2009 Tenth International Conference on Mobile Data Management: Systems, Services and Middleware, IEEE, 2009, pp. 692–697.
[33] F. Biljecki, H. Ledoux, J. Stoter, An improved lod specification for 3d building models, Comput. Environ. Urban Syst. 59 (2016) 25–37.
[34] T. Kutzner, K. Chaturvedi, T.H. Kolbe, Citygml 3.0: new functions open up new applications, Journal of Photogrammetry, Remote Sensing and Geoinformation Science 88 (1) (2020) 43–61.
[35] D. Crawley, L. Lawrie, Climate.onebuilding.org, https://climate.onebuilding.org/default.html. (Accessed 25 March 2022), 2019.
[36] G. Quek, J.A. Jakubiec, Calibration and validation of climate-based daylighting models based on one-time field measurements: office buildings in the tropics, Leukos 17 (1) (2021) 75–90.
[37] C.L. Guide, 10: Daylighting and window design, CIBSE, 1999.
[38] M.A. Stephens, Edf statistics for goodness of fit and some comparisons, J. Am. Stat. Assoc. 69 (347) (1974) 730–737.
[39] R. D'AGOSTINO, E.S. Pearson, Tests for departure from normality. Empirical results for the distributions of b 2 and√ b, Biometrika 60 (3) (1973) 613–622.
[40] G.W. Larson, R. Shakespeare, Rendering with Radiance: the Art and Science of Lighting Visualization, Morgan Kaufmann Publishers Inc., 1998.
[41] D. Geisler-Moroder, E.S. Lee, G.J. Ward, Validation of the five-phase method for simulating complex fenestration systems with radiance against field measurements, Tech. Rep., Lawrence Berkeley National Lab. (LBNL), Berkeley, CA (United States), 2016.
[42] A. McNeil, C. Jonsson, D. Appelfeld, G. Ward, E.S. Lee, A validation of a ray-tracing tool used to generate bi-directional scattering distribution functions for complex fenestration systems, Sol. Energy 98 (2013) 404–414.
[43] J. Mardaljevic, Validation of a lighting simulation program under real sky conditions, Int. J. Light. Res. Technol. 27 (4) (1995) 181–188.
[44] S. Subramaniam, Daylighting Simulations with Radiance Using Matrix-Based Methods, Lawrence Berke-Ley National Laboratory, 2017.
[45] N. Forouzandeh Shahraki, E. Brembilla, J.A. Jakubiec, Image-based material characterization for daylight simulation using illuminance-proxy and artificial neural networks, in: Proceedings of the 14th European Lighting Conference LUX EUROPA, 2022.
[46] J. Mardaljevic, E. Brembilla, N. Drosou, Illuminance-proxy high dynamic range imaging: a simple method to measure surface reflectance, 2015.
[47] CIBSE, Lighting guide lg10, Chartered Institution of Building Services Engineers, 1999.